Sascha Lüdeke*, Vanessa Wyrwoll, Tenzin S. Stelljes, Hui Khee Looe, Dietrich Harder and Björn Poppe

Determination of EPID convolution kernels for portal imaging using carbon target bremsstrahlung

Abstract: Improving the accuracy and reproducibility during patient positioning is of paramount importance. Hence, the goal of this work is to characterize the aspects of image blurring occurring during carbon target bremsstrahlung portal imaging and to assess the applicability of a deconvolution algorithm. Blurring effects involved in this method of portal imaging are electron scattering inside the EPID, geometric blurring due to the photon source size and photon scattering inside the patient. These effects can all be described by convolutions using as the convolutional kernel a Lorentz function, whose FWHM is 2λ. The λ values measured for these effects range from 0.2 mm to 0.45 mm, and an iterative 2D-deconvolution of carbon target portal images was performed accordingly. A significant decrease in the image blurring of test objects has been achieved and confirmed by analyzing the RMTF. However for clinical images, the deconvolution method is presently faced with the problem of the associated increase of image noise.

Keywords: EPID, deconvolution, portal imaging, carbon target, iterative

https://doi.org/10.1515/cdbme-2017-0046

1 Introduction

Due to the high relevance of reproducibility and accuracy during patient positioning in radiotherapy, this work aims to improve portal imaging using carbon target bremsstrahlung provided by the Siemens Artiste linac. To achieve this the 2D iterative deconvolution algorithm proposed by [1] is used. Therefore, the convolution kernel of the electronic portal imaging device (EPID) must be determined for the bremsstrahlung radiation spectrum provided by the carbon target. The deconvolution algorithm was applied to EPID images of a TOR 18FG line phantom (Leeds Test Objects LTD, UK) and to clinical images to evaluate its effectiveness.

2 Materials and methods

2.1 Linear accelerator and EPID

The Siemens Artiste linear accelerator is equipped with an additional carbon target providing the possibility to generate a softer radiation spectrum with a nominal energy of 1 MV to increase the contrast of portal images. The facility is equipped with an EPID (Optivue 1000ST, Siemens, Concord, CA, USA) [1], whose active detector area spans 41 cm by 41 cm with a matrix of 1024 by 1024 pixels. The detection layer of the EPID is shielded by a 1 mm copper layer preventing secondary electrons to reach the sensitive layer from the outside and creating new electrons to generate the signal of the detector. The generation of an EPID image requires a dose to the patient at 10 cm depth of the order of 10 mGy.

2.2 The convolution kernel K(x,y)

2.2.1 Mathematical model

As described in [1] the 2D convolution kernel of the EPID is a Lorentz function with width parameter λ:

***Corresponding author: Sascha Lüdeke:** Pius-Hospital Oldenburg, Germany, e-mail: sascha.luedeke@uni.oldenburg.de
Vanessa Wyrwoll, Tenzin S. Stelljes, Hui Khee Looe, Björn Poppe: Pius-Hospital Oldenburg, Germany
Dietrich Harder: Georg-August-Universität Göttingen, Germany

$$\mathbf{K(x,y)} = \frac{1}{\left(1+\frac{x^2+y^2}{\lambda^2}\right)^{\frac{3}{2}}} \quad (1)$$

To determine the different contributions to the convolution kernel we used the 1D edge spread function (ESF):

$$\mathbf{ESF(x)} = \frac{1}{\pi}\left[\frac{\pi}{2} + \boldsymbol{tan^{-1}}\left(\frac{x}{\lambda}\right)\right] \quad (2)$$

and the Fourier transform of the 1D kernel:

$$\mathbf{FT[K}(\boldsymbol{x})] = \boldsymbol{exp}(-\mathbf{2}\boldsymbol{\pi\nu_x\lambda}) \quad (3)$$

2.2.2 Measurements of λ

2.2.2.1 Secondary electron transport

The contribution of secondary electron transport inside the EPID to the convolution kernel was evaluated with a lead block placed directly on the EPID during the measurement. The measured ESF defined by the lead block was then fitted with the expected ESF (see equation 2) to determine λ.

2.2.2.2 Geometric blurring

Due to the finite size of the photon source the penumbra of the beam provides additional blurring. This blurring aspect is also described by the convolution kernel (see equation (1)). Therefore, the ESF of the lead edge was measured at different focus detector distances (FDD) and focus edge distances (FED). The values for FDD were 140 cm, 145 cm, 150 cm and 92.5 cm, 100 cm, and 107.5 cm for FED. The measurements were solely done in inplane direction as Looe *et al.* [1] showed that the blurring is independent of plane direction. Afterwards the measurements were repeated with the edge embedded in RW3.

2.2.2.3 Phantom scattering

To investigate the blurring caused by phantom material, e.g. the patient, a 15 x 300 mm² slit beam was measured with and without 30 cm RW3 above the EPID. The two measurements were used to determine the width of the convolution kernel based on the method proposed in [2]. On the basis of equation 4 in which S_{30} indicates the signal with 30 cm phantom material and S_0 the signal without material

$$\mathbf{FT}[\boldsymbol{S_{30}(x)}] = \boldsymbol{FT}[\boldsymbol{S_0(x)}] \,\mathbf{x}\, \boldsymbol{FT}[\boldsymbol{K(x)}] \quad (4)$$

the Fourier transform of the convolution Kernel can be determined by plotting the ratio $\mathbf{FT}[\boldsymbol{S_{30}(x)}]/\boldsymbol{FT}[\boldsymbol{S_0(x)}]$ over the spatial sampling frequency $\boldsymbol{\nu_x}$ and using equation (3).

2.3 The deconvolution algorithm

The deconvolution algorithm used in this work is based on the algorithm described in [1].

2.4 Application of the deconvolution algorithm

Finally, the deconvolution algorithm was applied to portal images of the TOR 18FG phantom taken with the carbon target radiation. To quantify the improvement of the images by the algorithm the relative modulated transfer function (RMTF) was calculated. Afterwards the algorithm was applied to clinical images.

3 Results

3.1 Secondary electron transport

The results for the ESF created by the secondary electron transport inside the EPID are displayed in Fig. 1. The measured ESF shows good agreement with a fitted Lorentz function having a width parameter of λ=0.31 mm for an FDD of 150 cm.

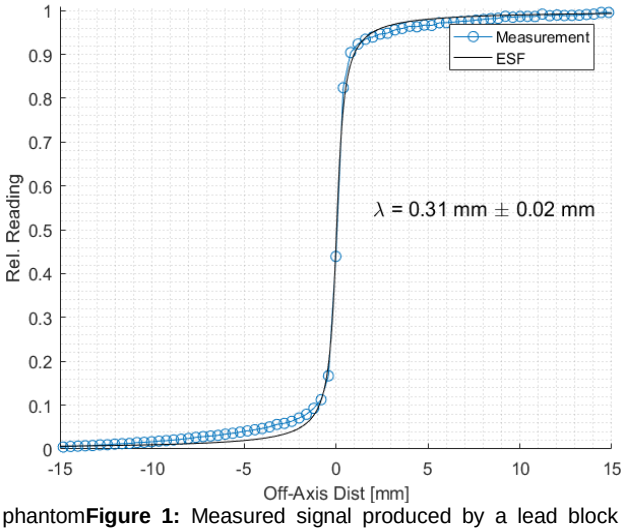

phantom**Figure 1:** Measured signal produced by a lead block placed on the EPID. The fitted ESF is based on (2).

3.2 Geometric blurring

Fig. 2 shows the determined λ values for the geometric blurring due to the finite source size of the accelerator. These values are displayed in Fig. 2 as a function of the magnification factor given in equation (5):

$$\frac{\mathbf{FED-FDD}}{\mathbf{FDD}} = \frac{\mathbf{FED}}{\mathbf{FDD}} - \mathbf{1} \tag{5}$$

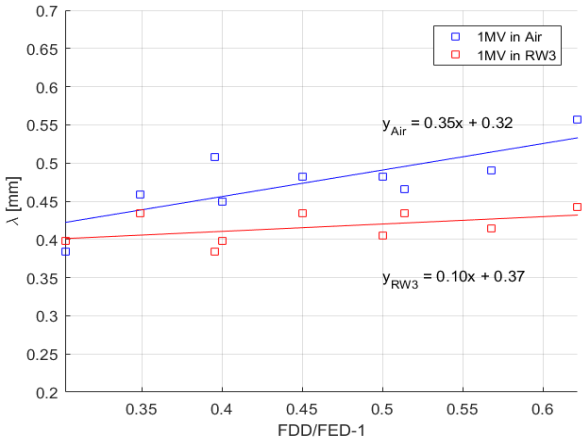

Figure 2: λ values determined for the geometric blurring plotted against the magnification factor

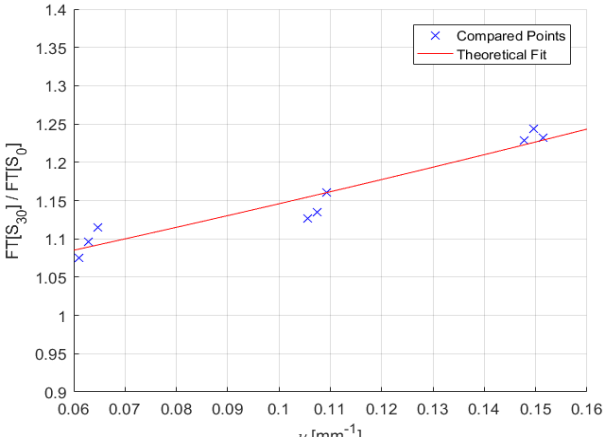

Figure 3: Determination of the deconvolution kernel for the image blurring due to phantom scattering using (4).

The λ values were determined in the same way as in 3.1 by fitting the ESF to the measured edge profiles. Again, the measurements were in good agreement with the mathematical model. The data show an increase of the width of the Lorentz kernel with greater magnification. This increase is more noticeable when the edge is not surrounded by RW3 phantom material. Overall, the change of λ in the clinical magnification range is negligible and therefore static values of 0.45 mm in air and 0.42 in RW3 will be applied for the deconvolution algorithm.

3.3 Phantom scattering

The calculation of λ for the phantom scattering kernel yielded an absolute value of λ=0.22 mm. The result of the fit using equation (3) can be seen in Fig. 3.

3.4 Application of the deconvolution algorithm

The original portal image of the line phantom is shown in Fig. 4 and the deconvolved image in Fig.5. The result of the calculated RMTFs are shown in Fig. 6. The RMTFs show that the deconvolution algorithm reduces the lowpass filtering aspect of the convolution kernel. The RMTF of the deconvolved image shows higher high frequency components

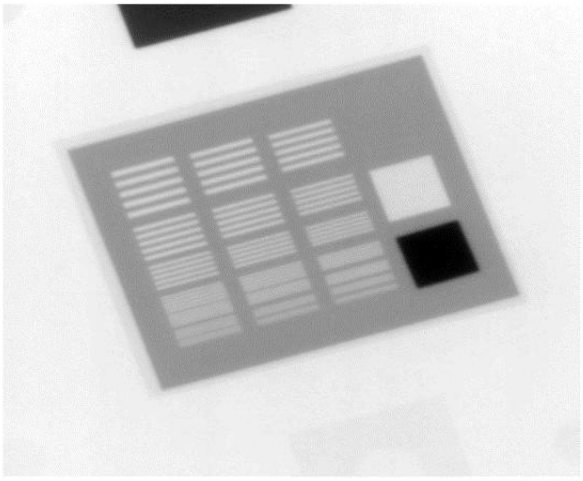

Figure 4: Original 1 MV portal image of the line phantom

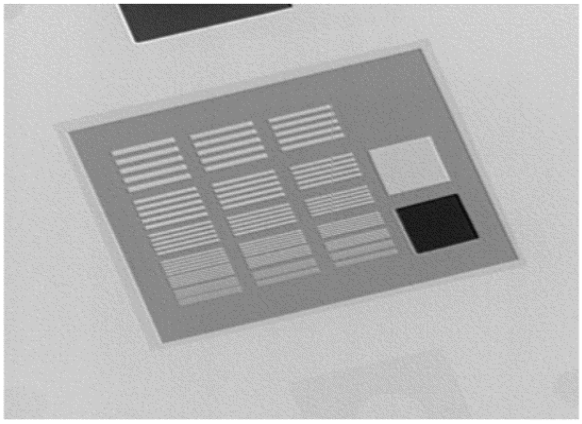

Figure 5: Deconvolved 1 MV portal image of the line

compared to the original image. Additionally, the deconvolution algorithm decreases the contrast of the image.

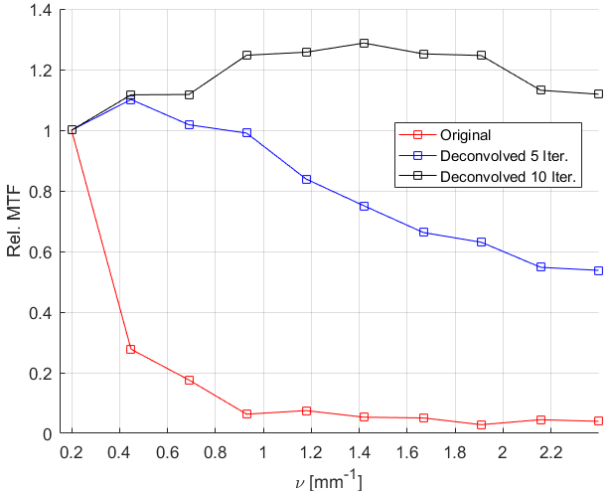

Figure 6: RMTF for the original image, the deconvolved image using 5 and 10 iterations

3.4.1 Deconvolution of clinical images

The original and deconvolved clinical images of a pelvis can be seen in Fig. 7 and Fig. 8 respectively. The deconvolution decreases the blurring of the image, but both images show

Figure 7: Original 1 MV portal image of a pelvis

great amounts of noise, which is further amplified by the deconvolution, although the noise was reduced by smoothing the original image before the deconvolution and the resulting image again after application of the algorithm. Furthermore, the image loses contrast after the deconvolution.

Figure 8: Deconvolved 1 MV portal image of a pelvis

4 Discussion

The evaluation of carbon target bremsstrahlung portal images showed that the characteristics proven for 6 MV and 15 MV portal images by [1] are also present in 1 MV portal images. The contributions to the image blurring can be described using Lorentz functions, and the deconvolution algorithm described in [1] can be used to reduce blurring of the portal images. The results of the deconvolution of a line phantom image were satisfying. However, the clinical images suffer from strong noise pollution, and the image quality so far achieved by deconvolution shows noise amplification and a loss of contrast. This may partly be due to the fact that the original images already comprise edge enhancement.

5 Conclusion

For the contrast-rich portal images achieved with the carbon target of the Siemens Artiste accelerator, we have shown the applicability of image blurring reduction by iterative image deconvolution. While satisfying results have been achieved with a line phantom, the deconvolved clinical portal images still suffer from noise enhancement and contrast reduction. The possibilities of noise reduction available during data acquisition and image pre-processing will be investigated in further work.

Author's Statement

Research funding: The authors state no funding involved. Conflict of interest: Authors state no conflict of interest. Informed consent: Informed consent is not applicable. Ethical approval: The conducted research is not related to either human or animals use.

References

[1] Looe H K, Harder D, Willborn K, Poppe B. Iterative 2D deconvolution of portal imaging radiographs. Z Med Phys 2011; 21:52-64

[2] Djouguela A, Harder D, Kolhoff R, Foschepoth S, Kunth W, Rühmann A, Wollborn K, Poppe B. Fourier deconvolution reveals the role of the Lorentz function as the convolution kernel of narrow photon beams. Phys Med Biol 2009; 54:2807-27